Pyroptosis and Necroptosis Inhibitor Necrosulfonamide Prevents Lipopolysaccharide-Induced Inflammatory Hyperalgesia in Mice

Beyza Ozgen
Mersin University
Sefika Pinar Senol
Tarsus University
Dilsah Ezgi Yilmaz
Mersin University
Meryem Temiz-Resitoglu
Mersin University
Omer Bahceli
Mersin University
Bahar Tunctan (btunctan@gmail.com)
Mersin University

Research Article

Keywords: Lipopolysaccharide, Necrosulfonamide, Inflammatory hyperalgesia, Pyroptosis, Necroptosis.

Posted Date: June 13th, 2022

DOI: https://doi.org/10.21203/rs.3.rs-1727695/v1

Abstract

Recent studies have demonstrated that two distinct forms of necrotic cell death, pyroptosis, and necroptosis, triggered by the lipid A part of lipopolysaccharide (LPS) are involved in the pathogenesis of several neurodegenerative diseases associated with neuroinflammation. It has been suggested that inhibition of gasdermin D (GSDMD)-mediated pyroptosis and/or mixed lineage kinase domain-like pseudokinase (MLKL)-mediated necroptosis may have a therapeutic potential in the treatment of inflammatory diseases of the central nervous system (CNS). However, the involvement of both types of cell death in LPS-induced inflammatory hyperalgesia remains unknown. Therefore, we aimed to investigate whether GSDMD and MLKL inhibitor, necrosulfonamide (NSA), prevents inflammatory hyperalgesia induced by LPS via inhibiting caspase-11/GSDMD-mediated pyroptosis and receptor-interacting serine/threonine-protein kinase (RIPK) 1/RIPK3/MLKL-mediated necroptosis in the CNS of mice. It was observed that 6 hours after intraperitoneal (i.p.) injection of LPS (10 mg/kg), the response time of mice to thermal stimulation determined by hot plate test was prevented with 0.01, 0.1, and 1 mg/kg (i.p.) doses of NSA. When NSA was administered at the lowest effective dose (0.01 mg/kg), it prevented the LPS-induced increase in caspase-11 p20, p30-GSDMD, interleukin-1β, high-mobility-group-box 1, and semaphorin (SEMA) protein expression as well as activity of RIPK1, RIPK3, and MLKL associated with decreased expression of myelin proteolipid protein (PLP) in the tissues of LPS-treated mice. Our findings suggested a decrease in the caspase-11/GSDMD-mediated pyroptosis, RIPK1/RIPK3/MLKL necrosome-mediated necroptosis, and remyelination inhibitor, SEMA3A, as well as increased expression of the main protein of the CNS myelin membrane, PLP, in the CNS of mice involves in the protective effect of NSA against inflammatory hyperalgesia induced by LPS.

Introduction

Several programed cell death pathways have become known to be associated with innate immunity, including apoptosis, pyroptosis, necroptosis, ferroptosis, and PANoptosis in recent decades [1–8]. Recent studies have provided an evidence that two distinct forms of necrotic cell death, particularly caspase-11-mediated pyroptosis and mixed lineage kinase domain-like pseudokinase (MLKL)-mediated necroptosis, triggered by toll-like receptor (TLR) 4 ligands such as lipopolysaccharide (LPS) are involved in the pathogenesis of several diseases in particular neurodegenerative diseases associated with neuroinflammation [8–12].

The non-canonical inflammasome, comprising inflammatory caspases, caspase-11 in rodents (caspase 4 and 5 in human), detects bacterial components including lipid A component of LPS, endotoxin, of Gram-negative bacteria [5, 9, 12–14]. Upon activation by cytosolic Gram-negative bacteria or intracellular LPS, caspase-11 as an intracellular LPS receptor undergoes oligomerization and next cleaves its substrate, gasdermin D (GSDMD) into pore-forming peptides (i.e., the catalytic N-terminal domain of GSDMD, p30-GSDMD) [15]. GSDMD pore formation leads to the pyroptosis, a lytic programed cell death and the release of pro-inflammatory cytokines including interleukin (IL)-1β and damage-associated molecular

patterns (DAMPs), such as high-mobility-group-box (HMGB) 1, thereby promoting inflammatory responses by regulating both the innate and the adaptive immune responses [16].

LPS can also induce necroptosis, a caspase-independent inflammatory form of regulated cell death caused by necrosis [4, 6, 17]. This type of necrotic cell death involves formation of the receptor-interacting kinase 1 (RIPK1)/RIPK3 necrosome leading to activation of the MLKL through its phosphorylation [18]. Following activation of MLKL molecules, they oligomerize and translocate to the cell membrane where they compose cation-selective ion channels. The generated ionic disturbance leads to the swelling of cells and organelles, rupture of the plasma membrane, and release of DAMPs, including HMGB1 [19].

Inhibition of GSDMD-mediated pyroptosis and/or MLKL-mediated necroptosis has currently emerged as a therapeutic target in the treatment of various neuroinflammatory neurodegenerative central nervous system (CNS) diseases including Alzheimer's disease [4, 6, 20, 21], amyotrophic lateral sclerosis [6, 22], Huntington's disease [6, 20], multiple sclerosis [6], and Parkinson's disease [6, 20]. The results of a few studies published to date emphasize that GSDMD and MLKL inhibitor, necrosulfonamide (NSA), which can also enter the CNS when administered systemically [23, 24], may represent a promising therapeutic agent for reducing neuroinflammation and accelerating anti-inflammatory responses through protective mechanisms potentially related to inhibition of pyroptotic and necroptotic signaling pathways as demonstrated in the animal models of systemic inflammation [15, 24–28]. It has also been reported that the effects of LPS on pyroptosis [15, 29, 30] and necroptosis [31–33] *in vitro* and *in vivo* is reversed by NSA. However, there are no studies focusing on either the role of both types of cell death or the effect of NSA in perceived LPS-induced inflammatory hyperalgesia at the spinal and/or supraspinal level remains unknown.

LPS has been shown to enhance pain sensation in response to thermal stimuli at spinal and supraspinal levels, as indicated by the hot plate test, which is considered an integration of supraspinal pathways [34, 35]. In our previous studies, we demonstrated that inflammatory hyperalgesia induced by LPS is associated with decreased expression and/or activity of inducible nitric oxide (NO) synthase (NOS), neuronal NOS, NLRC3, soluble epoxide hydrolase, and peroxisome proliferator-activated receptors α/β/γ in the brain and spinal cord of mice [36–40]. Enhanced activity of canonical NLRC4/ASC/pro-caspase-1, and non-canonical caspase-11 inflammasomes, nucleotide-binding domain and leucine-rich repeat protein (NLRP3)/apoptosis-associated speck-like protein containing caspase activation and recruitment domain (ASC)/pro-caspase-1, TLR4/MyD88/transforming growth factor-activated kinase 1/NF-κB/cyclooxygenase (COX)-2, and NLRX1/TRAF6/IKK/IκB-α/NF-κB pathways, and nicotinamide adenine dinucleotide phosphate oxidase, which are associated with the formation of pro-inflammatory cytokines resulted in inflammation, were also observed in the CNS of LPS-treated mice [36–41]. Given the detrimental role of pyroptosis and necroptosis in inflammation, we aimed to investigate whether NSA prevents inflammatory hyperalgesia associated with demyelination induced by LPS via inhibiting caspase-11/GSDMD-mediated pyroptosis and RIPK1/RIPK3/MLKL-mediated necroptosis in the CNS of mice.

Materials And Methods

Animals

Balb/c mice (male; 20 to 30 g; *n* = 70) (Research Center of Experimental Animals, Mersin University, Mersin, Turkey) were used in the experiments. The mice were housed under a 12-hours light/dark cycle and fed on standard chow. The procedures on animals were approved by the Mersin University Experimental Animals Local Ethics Committee (Approval date: June 28, 2021; Protocol number: 2021/31) and performed following the National Institutes of Health Guide for the Care and Use of Laboratory Animals.

Inflammatory Hyperalgesia Model

The inflammatory hyperalgesia model was induced by intraperitoneal injection of LPS, and the latency of pain to nociceptive response was evaluated by the hot plate test as previously reported [37–40, 42]. Mice were randomly divided into 8 groups, and the dose-response relationship was investigated with different NSA doses to observe the pain behavior [15, 24, 26, 28]: (1) Saline (10 ml/kg), (2) LPS (10 mg/kg; 10 ml/kg; intraperitoneal [i.p.]), (3) saline + dimethyl sulfoxide (DMSO) (10 ml/kg; i.p.), (4) saline + NSA (0.01 mg/kg; 10 ml/kg; i.p.), (5) LPS + NSA (0.001 mg/kg; 10 ml/kg; i.p.), (6) LPS + NSA (0.01 mg/kg; 10 ml/kg; i.p.), (7) LPS + NSA (0.1 mg/kg; 10 ml/kg; i.p.), and (8) LPS + NSA (1 mg/kg; 10 ml/kg; i.p.). DMSO (60153; A1584; Applichem GmbH, Darmstadt, Germany), NSA (dissolved in 6% DMSO; 480073; Sigma Chemical Co., St. Louis, MO, USA) was injected into the mice simultaneously with saline or LPS (dissolved in saline; L4130; *Escherichia coli* LPS, O111:B4; Sigma). Mice treated with saline, LPS, or DMSO were used as control, inflammatory hyperalgesia, and vehicle control groups, respectively. Mice were placed individually on a plate pre-heated to 55 ± 0.2°C (AHP 9601, Commat Ltd., Ankara, Turkey). The latency to paw withdrawal within 30 seconds was recorded using the hot plate test after the mice showed the first signal of paw licking 6 hours thereafter administration of saline, LPS, and/or NSA. According to our previous time-course studies [40], the time point of 6 hours was chosen for the assessment of hyperalgesia. Mice were euthanized after the test by cervical dislocation and exsanguination, and the brains and spinal cords of the animals were collected.

Immunoblotting Studies

The immunoblotting method was used according to the protocol as described in detail previously with minor modifications [37–39]. Briefly, tissue homogenates (30 µg of protein) were subjected to a 10% sodium dodecyl sulfate-polyacrylamide (SDS-PAGE) (10%) gel electrophoresis. After electrophoresis was complete, proteins were transferred from the gel to the nitrocellulose membranes. The membranes were blocked with non-fat dry milk in Tris-buffered saline and incubated with primary antibodies against (1) caspase-11 p20 (sc-374615; Santa Cruz Biotechnology, Santa Cruz, CA, USA), (2) p30-GSDMD (sc-393656; Santa Cruz), (3) IL-1β (sc-52012; Santa Cruz), (4) HMGB1 (sc-sc-56698; Santa Cruz), (5) RIPK1 (ARG55746; Arigo Biolaboratories, Hsinchu City, Taiwan), (6) phosphorylated RIPK1 (p-RIPK1) (ARG66476; Arigo Biolaboratories), (7) RIPK3 (PA5-19956; Thermo Fisher, Waltham, MA USA), (8)

phosphorylated RIPK3 (p-RIPK3) (PA5-105701; Thermo Fisher), (9) MLKL (PA5-102810; Thermo Fisher), (10) phosphorylated MLKL (p-MLKL) (PA5-102810; Thermo Fisher), (11) SEMA3A (sc-74554; Santa Cruz), and (12) myelin PLP (bs-11093R-HRP; Bioss Antibodies Inc., Woburn, MA, USA) in bovine serum albumin (BSA) overnight at 4°C. The membranes were then incubated with appropriate secondary antibodies (sheep anti-mouse [RPN4201; Amersham Life Sciences, Cleveland, OH, USA] or goat anti-rabbit IgG-horseradish peroxidase [RPN4301; Amersham]) in BSA at room temperature for 1 h. The immune complexes were detected by ECL Prime Western Blotting Detection Reagent (RPN2232; Amersham) according to the manufacturer's instructions. The photos of the immunoreactive bands were captured with a gel-imaging system (EC3-CHEMI HR imaging system; Ultra-Violet Products, UVP, Cambridge, UK). To determine the relative immunoreactive densities of bands, Image J densitometry analysis software (Image J 1.53k, Wayne Rasband, National Institutes of Health, Bethesda, MD, USA) was used. The membranes were reused for anti-β-tubulin antibody (sc-5274; Santa Cruz) as a loading control. The ratio of each band/β-tubulin was taken into account for the expression level of specific proteins.

Statistical Analysis

The sample size determined for each treatment group in each experiment was based on previous studies from our laboratory [36–40] and complied with power analysis [43]. The results are expressed as means ± standard error of the mean (SEM). For data normally distributed, parametric statistical analysis was conducted using one-way analysis of variance followed by Student-Newman-Keuls test for multiple comparisons to assess whether there is a significant difference between the mean values of β-tubulin in each group. For data normally or not normally distributed, parametric or nonparametric statistical analysis was performed with Student's *t*-test or Mann-Whitney *U*-test for normally or nonnormally distributed data, respectively. Statistical analysis was performed using GraphPad Prism version 7.04 for Windows (GraphPad Software, San Diego California USA; http://www.graphpad.com). $p < 0.05$ was considered to indicate a statistically significant difference.

Results

NSA Treatment Prevents Hyperalgesia Induced by LPS

To test the effect of NSA on LPS-induced hyperalgesia, NSA was injected into mice alone or in combination with saline or LPS. LPS caused a decrease in the hot plate latency 6 hours thereafter LPS injection compared with control group values (Fig. 1) ($p < 0.05$). NSA at doses of 0.01, 0.1, and 1 mg/kg prevented the reduction in latency compared with LPS-injected mice ($p < 0.05$). NSA at the dose of 0.001 mg/kg was ineffective in preventing the decrease in latency compared with the LPS-injected mice ($p > 0.05$). At a dose of 0.01 mg/kg, treatment with NSA had no effect on hot plate latency in mice treated with saline or DMSO ($p > 0.05$). No mortality was also observed during the study. Accordingly, tissues from mice injected with NSA at the minimum effective dose (0.01 mg/kg) in LPS-induced hyperalgesia were used for further experiments.

NSA Treatment Prevented the LPS-Induced Increase in Caspase-11/GSDMD-Mediated Pyroptosis

To test the effect of NSA on the LPS-induced caspase-11/GSDMD-mediated pyroptosis in the CNS, the brain and spinal cord tissue samples of saline-, LPS-, DMSO-, and/or NSA-treated mice were immunoblotted with specific caspase-11 p20, p30-GSDMD, IL-1β, and HMGB1 antibodies. Increased expression of caspase-11 p20, p30-GSDMD, IL-1β, and HMGB1 was observed in the brains (Fig. 2a-d) and spinal cords (Fig. 2e-h) of LPS-injected mice compared with the levels in the control group values ($p < 0.05$). Treatment with NSA inhibited the LPS-induced increase in caspase-11 p20, p30-GSDMD, IL-1β, and HMGB1 expression in tissues compared with LPS-injected mice ($p < 0.05$). The expression of these proteins in the tissues of NSA-treated mice was not different from the control group ($p > 0.05$).

NSA Treatment Prevented the LPS-Induced Increase in RIPK1/RIPK3/MLKL Necrosome-Mediated Necroptosis

To investigate the effect of NSA on the LPS-induced RIPK1/RIPK3/MLKL necrosome-mediated necroptosis in the CNS, the brain and spinal cord tissue samples of saline-, LPS-, DMSO-, and/or NSA-treated mice were immunoblotted with specific antibodies for RIPK1, p-RIPK1 (at Ser^{166}), RIPK3, p-RIPK3 (at Ser^{232}), MLKL, and p-MLKL (at Ser^{358}). Increased expression of the p-RIPK1, p-RIPK3, and p-MLKL, but not RIPK1, RIPK3, and MLKL proteins was observed in the brains (Fig. 3a-c) and spinal cords (Fig. 3d-f) of LPS-injected mice compared with levels in the control group values ($p < 0.05$). Treatment with NSA inhibited the LPS-induced increase in the p-RIPK1, p-RIPK3, and p-MLKL expression in tissues compared with LPS-injected mice ($p < 0.05$). The expression of unphosphorylated and phosphorylated proteins in the tissues of NSA-treated mice was not different from the control group ($p > 0.05$).

NSA Treatment Prevented the LPS-Induced Increase in SEMA3A Expression

To investigate the effect of NSA on the expression of SEMA3A in the CNS, the brain and spinal cord tissue samples of saline-, LPS-, DMSO-, and/or NSA-treated mice were immunoblotted with a specific SEMA3A antibody. Increased expression of SEMA3A was observed in the brains (Fig. 4a) and spinal cords (Fig. 4b) of LPS-injected mice compared with levels in the control group ($p < 0.05$). Treatment with NSA inhibited the LPS-induced increase in SEMA3A expression in tissues compared with LPS-injected mice ($p < 0.05$). The expression of SEMA3A in the tissues of NSA-treated mice was not different from the control group ($p > 0.05$).

NSA Treatment Prevented the LPS-Induced Decrease in Myelin PLP Expression

To investigate the effect of NSA on the expression of myelin PLP in the CNS, the brain and spinal cord tissue samples of saline-, LPS-, DMSO-, and/or NSA-treated mice were immunoblotted with a specific myelin PLP antibody. Decreased expression of myelin PLP was observed in the brains (Fig. 5a) and

spinal cords (Fig. 5b) of LPS-injected mice compared with levels in the control group ($p < 0.05$). Treatment with NSA inhibited the LPS-induced decrease in myelin PLP expression in tissues compared with LPS-injected mice ($p < 0.05$). The expression of myelin PLP in the tissues of NSA-treated mice was not different from the control group ($p > 0.05$).

Discussion

The results of this study indicate, for the first time, that GSDMD and MLKL inhibitor, NSA, prevents hyperalgesia through inhibiting increased protein expression of caspase-11 p20, p30-GSDMD, IL-1β, HMGB1, and SEMA3A in addition to RIPK1, RIPK3, and MLKL phosphorylation associated with decreased myelin PLP expression in the CNS of LPS-treated mice. Consistent with our previous findings [36–40], the results of the present study provide the first evidence that NSA prevents LPS-induced inflammatory hyperalgesia by not only inhibiting caspase-11/GSDMD-mediated pyroptosis, RIPK1/RIPK3/MLKL necrosome-mediated necroptosis, and demyelination but also promoting remyelination in the CNS of mice (Fig. 6).

Systemic administration of NSA has been shown to be efficacious in several inflammatory rodent models *in vivo* including LPS-induced sepsis in mice [15], $AlCl_3$-induced Alzheimer's disease in rats [26], ischemia-reperfusion injury in rats [27], spinal cord injury in mice [24] and rats [28], and post-resuscitation myocardial dysfunction in mice [25] through protective mechanisms potentially related to inhibition of GSDMD-dependent pyroptotic and MLKL-dependent necroptotic pathways. In only one study conducted to date, Rathkey et al. [15] demonstrated that NSA (20 mg/kg; i.p.) binds directly to GSDMD and can ameliorate GSDMD-driven mortality associated with increased serum IL-1β and IL-6 levels in murine sepsis induced by LPS (25 mg/kg; i.p.). Nevertheless, to the best of our knowledge, the effect of NSA on LPS-induced inflammatory hyperalgesia has not been investigated. Increasing evidence also suggests that caspase-11/GSDMD-mediated pyroptosis signaling pathway triggered by LPS plays an important role in the pathogenesis of neuroinflammatory disorders [44, 45]. Although NSA has been shown to reverse the effects of LPS on pyroptosis both *in vitro* and *in vivo* [15, 29, 30]; its effects on caspase-11/GSDMD-mediated pyroptosis in the CNS during LPS-induced inflammatory hyperalgesia remain unknown. In the present study, we showed that systemic administration of LPS into mice resulted in hyperalgesia as well as increased protein expression of caspase-11 p20, p30-GSDMD, IL-1β, and HMGB1 in the mouse brain and spinal cord. Therefore, in agreement with the results of previous studies [15, 46] and our previous findings [36–40], this study presents novel data suggesting that NSA prevents hyperalgesia through decreased formation of pro-inflammatory mediators and HMGB1 release by pyroptotic cells to promote inflammation as a result of cell rupture and pyroptosis as a result of suppressed expression and/or activity of the caspase-11/GSDMD-mediated pyroptotic pathway. These findings also suggest that not only binding directly to GSDMD to inhibit p30-GSDMD oligomerization and pyroptosis, but also directly or indirectly decreasing expression of caspase-11 p20, p30-GSDMD, IL-1β, and HMGB1 proteins in the CNS of LPS-treated mice contribute to the protective effect of NSA in the

hyperalgesia model. However, additional studies should be done to prove the validity of these hypotheses.

Recent evidence also indicates that RIPK1/RIPK3/MLKL necrosome-mediated necroptosis plays a crucial role in the pathogenesis of LPS-induced models of neuroinflammation-related CNS disorders [47–51]. There are only a few studies in the literature showing that NSA reverses the effects of LPS on the changes in the expression and/or activity of key components of necroptosis, RIPK1, RIPK3, and MLKL, *in vitro* [31–33]. On the other hand, it is unknown whether NSA prevents LPS-induced RIPK1/RIPK3/MLKL necrosome-mediated necroptosis in the CNS during inflammatory hyperalgesia. In the current study, we demonstrated that systemic administration of LPS into mice also resulted in not only increased phosphorylation of RIPK1, RIPK3, and MLKL proteins but also HMGB1 protein expression in the brain and spinal cord tissues. These data suggest that HMGB1 released by necrotic cells to promote inflammation as a result of cell rupture and necrosis due to increased activity of the RIPK1/RIPK3/MLKL necrosome-mediated necroptotic pathway in the CNS of mice seems to be involved in inflammatory hyperalgesia induced by LPS. Our findings also suggest that not only binding directly to MLKL to inhibit MLKL oligomerization and necroptosis, but also directly or indirectly, decreasing phosphorylation of RIPK1, RIPK3, and MLKL proteins in the CNS of LPS-treated mice contributes to the protective effect of NSA in the hyperalgesia model. However, additional studies should be done to prove the validity of these hypotheses.

SEMA3A, one of the remyelination inhibitors, is reported to be increased in the mouse brain in response to intracerebroventricular injection of LPS [52]. In recent years, loss of myelin proteins such as PLP have also received major attention in the neuroinflammatory changes in the brain induced by systemic or intrauterin injection of LPS to rodents [53–55]. On the other hand, whether NSA prevents LPS-induced changes in the protein expression of SEMA3A and myelin PLP have not been investigated until recently. Consistent with the findings of previous studies [54, 55], we obtained additional evidence confirming that systemic administration of LPS into mice results in increased protein expression of SEMA3A associated with decreased myelin PLP expression in the mouse brain and spinal cords. Moreover, LPS-induced changes in the expression of SEMA3A and myelin PLP were reversed by NSA. These results suggest that NSA not only prevents demyelination but also promotes remyelination in the LPS-induced inflammatory hyperalgesia model in mice.

Collectively, in line with the above-mentioned studies and our previous findings, directly or indirectly decreased formation of pro-inflammatory mediators as a result of inhibition of caspase-11/GSDMD-mediated pyroptotic and RIPK1/RIPK3/MLKL necrosome-mediated necroptotic pathways at transcriptional and/or post-transcriptional level in the CNS seems to contribute to the preventive effect of NSA against LPS-induced enhanced pain sensitivity to thermal stimuli associated with demyelination. In addition, NSA may also exert its beneficial effects due to its synergistic effect on the signaling pathways that play a role in the pathogenesis of inflammatory hyperalgesia caused by LPS. Nevertheless, much more detailed experiments are needed to verify the validity of the proposed hypothesis. Hence, exploring molecular mechanisms of the effects of NSA on the LPS-induced inflammatory hyperalgesia associated

with demyelination in the CNS will ensure the framework for the extension of this research into comprehension the involvement of caspase-11/GSDMD-mediated pyroptosis and RIPK1/RIPK3/MLKL necrosome-mediated necroptosis. Therefore, further investigation will contribute to the preclinical and clinical studies to develop GSDMD and MLKL inhibitors, such as NSA, as drugs for the treatment of hyperalgesia-related demyelinating inflammatory diseases.

In conclusion, we demonstrated for the first time that the GSDMD and MLKL inhibitor, NSA, can prevent LPS-induced inflammatory hyperalgesia by preventing caspase-11/GSDMD-mediated pyroptosis, RIPK1/RIPK3/MLKL necrosome-mediated necroptosis, and demyelination in the CNS of mice. Thus, we suggest that GSDMD and MLKL inhibitors such as NSA may be useful as analgesic/anti-inflammatory drugs in the prevention and treatment of acute and chronic painful conditions in which inflammation plays a role in the pathophysiology that may result from bacterial infections.

Declarations

Acknowledgements: This study was supported by the Research Fund of Mersin University in Turkey with Project Number 2021-1-TP2-4393. The findings of this work were included in the Master's Thesis of Pharm. M.S. Beyza Ozgen.

AUTHOR CONTRIBUTION

B.T. conceptualized and conceived the research design, analyzed the data, and drafted the manuscript. B.T., B.O., S.P.S., M.T.R., and O.B. carried out the experiments. All authors read and approved the final manuscript.

FUNDING

This study was supported by the Research Fund of Mersin University in Turkey with Project Number 2021-1-TP2-4393.

DATA AVAILABILITY

Data supporting the results of this research are available to the corresponding author on request.

CODE AVAILABILITY

Not applicable.

Ethics approval All animal experiments were authorized by the Mersin University Experimental Animals Local Ethics Committee (Approval Date: June 28, 2021, Decision Number: 2021/31) and carried out according to the National Institutes of Health Guide for the Care and Use of Laboratory Animals.

Consent to Participate Not applicable.

Conflicts of Interest The authors declare that they have no conflict of interest.

References

1. Bertheloot, D., E. Latz, and B.S. Franklin. 2021. Necroptosis, pyroptosis and apoptosis: an intricate game of cell death. Cellular and Molecular Immunology 18(5): 1106–1121. https://doi.org/10.1038/s41423-020-00630-3.
2. Christgen, S., R.E. Tweedell, and T.D.Kanneganti. 2022. Programming inflammatory cell death for therapy. Pharmacology and Therapeutics 232: 108010. https://doi.org/10.1016/j.pharmthera.2021.108010.
3. Frank, D., and J.E. Vince. 2019. Pyroptosis versus necroptosis: similarities, differences, and crosstalk. Cell Death and Differentiation 26(1): 99–114. https://doi.org/10.1038/s41418-018-0212-6.
4. Gullett, J.M., R.E. Tweedell, and T.D. Kanneganti. 2022. It's all in the PAN: crosstalk, plasticity, redundancies, switches, and interconnectedness encompassed by PANoptosis underlying the totality of cell death-associated biological effects. Cells 11(9): 1495. https://doi.org/10.3390/cells11091495.
5. Lacey, C.A., and E.A. Miao. 2020. Programmed cell death in the evolutionary race against bacterial virulence factors. Cold Spring Harbor Perspectives in Biology 12(2): a036459. https://doi.org/10.1101/cshperspect.a036459.
6. Mázló, A., V. Jenei, S. Burai, T. Molnár, A. Bácsi, and G. Koncz. 2022. Types of necroinflammation, the effect of cell death modalities on sterile inflammation. Cell Death and Disease 13(5): 423. https://doi.org/10.1038/s41419-022-04883-w.
7. Miller, D.R., S.D. Cramer, A. Thorburn. 2020. The interplay of autophagy and non-apoptotic cell death pathways. International Review of Cell and Molecular Biology 352: 159–187. https://doi.org/10.1016/bs.ircmb.2019.12.004.
8. Yu, Z., N. Jiang, W. Su, Y. Zhuo. 2021. Necroptosis: a novel pathway in neuroinflammation. Frontiers in Pharmacology 12: 701564. https://doi.org/10.3389/fphar.2021.701564.
9. Burdette, B.E., A.N. Esparza, H. Zhu, and S. Wang. 2021. Gasdermin D in pyroptosis. Acta Pharmaceutica Sinica B 11(9): 2768–2782. https://doi.org/10.1016/j.apsb.2021.02.006.
10. Downs, K.P., H. Nguyen, A. Dorfleutner, and C. Stehlik. (2020) An overview of the non-canonical inflammasome. Molecular Aspects of Medicine 76: 100924. https://doi.org/10.1016/j.mam.2020.100924.
11. Jayaraman, A., and R. Reynolds. 2022. Diverse pathways to neuronal necroptosis in Alzheimer's disease. European Journal of Neuroscience Apr 4. https://doi.org/10.1111/ejn.15662.
12. Wright, S.S., S.O. Vasudevan, and V.A. Rathinam. 2022. Mechanisms and consequences of noncanonical inflammasome-mediated pyroptosis. Journal of Molecular Biology 434(4): 167245. https://doi.org/10.1016/j.jmb.2021.167245.

13. Abu Khweek, A., and A.O. Amer. 2020. Pyroptotic and non-pyroptotic effector functions of caspase-11. Immunological Reviews 297(1): 39–52. https://doi.org/10.1111/imr.12910.
14. Bezbradica, J.S., R.C. Coll, and D. Boucher. 2022. Activation of the non-canonical inflammasome in mouse and human cells. Methods in Molecular Biology 2459: 51–63. https://doi.org/10.1007/978-1-0716-2144-8_5.
15. Rathkey, J.K., J. Zhao, Z. Liu, Y. Chen, J. Yang, H.C. Kondolf, B.L. Benson, S.M. Chirieleison, A.Y. Huang, G.R. Dubyak, T.S. Xiao, X. Li, and D.W. Abbott. 2018. Chemical disruption of the pyroptotic pore-forming protein gasdermin D inhibits inflammatory cell death and sepsis. Science Immunology 3(26): eaat2738. https://doi.org/10.1126/sciimmunol.aat2738.
16. Heilig, R., M.S. Dick, L. Sborgi, E. Meunier, S. Hiller, and P. Broz. 2018. The gasdermin-D pore acts as a conduit for IL-1β secretion in mice. European Journal of Immunology 48: 584–592. https://doi.org/10.1002/eji.201747404.
17. Kang, T.B., S.H. Yang, B. Toth, A. Kovalenko, and D. Wallach. 2014. Activation of the NLRP3 inflammasome by proteins that signal for necroptosis. Methods in Enzymology 545: 67–81. https://doi.org/10.1016/B978-0-12-801430-1.00003-2.
18. Wang, H., L. Sun, L. Su, J. Rizo, L. Liu, L.F. Wang, F.S. Wang, and X. Wang. 2014. Mixed lineage kinase domain-like protein MLKL causes necrotic membrane disruption upon phosphorylation by RIP3. Molecular Cell 54(1): 133–146. https://doi.org/10.1016/j.molcel.2014.03.003.
19. Kolbrink, B., T. Riebeling, U. Kunzendorf, and S. Krautwald. 2020. Plasma membrane pores drive inflammatory cell death. Frontiers in Cell and Developmental Biology 8: 817. https://doi.org/10.3389/fcell.2020.00817.
20. Espinosa-Oliva, A.M., J. García-Revilla, I.M. Alonso-Bellido, and M.A. Burguillos. 2019. Brainiac caspases: beyond the wall of apoptosis. Frontiers in Cellular Neuroscience 13: 500. https://doi.org/10.3389/fncel.2019.00500.
21. Lee, S., H.J. Cho, and J.H. Ryu. 2021. Innate immunity and cell death in Alzheimer's disease. ASN Neuro 13: 17590914211051908. https://doi.org/10.1177/17590914211051908.
22. Neel, D.V., H. Basu, G. Gunner, and I.M. Chiu. 2022. Catching a killer: mechanisms of programmed cell death and immune activation in amyotrophic lateral sclerosis. *Immunological Reviews* May 7. https://doi.org/10.1111/imr.13083.
23. Bartzatt, R., S.L. Cirillo, and J.D. Cirillo. 2010. Sulfonamide agents for treatment of Staphylococcus MRSA and MSSA infections of the central nervous system. Central Nervous System Agents in Medicinal Chemistry 10(1): 84–90. https://doi.org/10.2174/187152410790780109.
24. Jiao, J., Y. Wang, P. Ren, S. Sun, and M. Wu. 2020. Necrosulfonamide ameliorates neurological impairment in spinal cord injury by improving antioxidative capacity. Frontiers in Pharmacology 10: 1538. https://doi.org/10.3389/fphar.2019.01538.
25. He, F., G. Zheng, J. Hu, W. Ge, X. Ji, J.L. Bradley, M.A. Peberdy, J.P. Ornato, and W. Tang. 2022. Necrosulfonamide improves post-resuscitation myocardial dysfunction via inhibiting pyroptosis and

necroptosis in a rat model of cardiac arrest. European Journal of Pharmacology 926: 175037. https://doi.org/10.1016/j.ejphar.2022.175037.

26. Motawi, T.M.K., Z.M. Abdel-Nasser, and N.N. Shahin. 2020. Ameliorative effect of necrosulfonamide in a rat model of Alzheimer's disease: targeting mixed lineage kinase domain-like protein-mediated necroptosis. ACS Chemical Neuroscience 11(20): 3386–3397. https://doi.org/10.1021/acschemneuro.0c00516.
27. Ueda, S., T.F. Chen-Yoshikawa, S. Tanaka, Y. Yamada, D. Nakajima, A. Ohsumi, and H. Date. 2022. Protective effect of necrosulfonamide on rat pulmonary ischemia-reperfusion injury via inhibition of necroptosis. Journal of Thoracic and Cardiovascular Surgery 163(2): e113-e122. https://doi.org/10.1016/j.jtcvs.2021.01.037.
28. Wang, Y., J. Wang, H. Wang, X. Feng, Y. Tao, J. Yang, and J. Cai. 2018. Necrosulfonamide attenuates spinal cord injury via necroptosis inhibition. World Neurosurgery 114: e1186-e1191. https://doi.org/10.1016/j.wneu.2018.03.174.
29. Li, Y., D. Song, F. Bo, M. Deng, and X. Tang. 2019. Diazepam inhibited lipopolysaccharide (LPS)-induced pyroptotic cell death and alleviated pulmonary fibrosis in mice by specifically activating GABAA receptor α4-subunit. Biomedicine and Pharmacotherapy 118: 109239. https://doi.org/10.1016/j.biopha.2019.109239.
30. Zhang, J., and K. Wei. 2021. Necrosulfonamide reverses pyroptosis-induced inhibition of proliferation and differentiation of osteoblasts through the NLRP3/caspase-1/GSDMD pathway. Experimental Cell Research 405(2): 112648. https://doi.org/10.1016/j.yexcr.2021.112648.
31. El-Mesery, M., A. Seher, T. Stühmer, D. Siegmund, and H. Wajant. 2015. MLN4924 sensitizes monocytes and maturing dendritic cells for TNF-dependent and -independent necroptosis. British Journal of Pharmacology 172(5): 1222–1236. https://doi.org/10.1111/bph.12998.
32. Geng, F., J. Liu, C. Yin, S. Zhang, Y. Pan, and H. Sun. 2022. Porphyromonas gingivalis lipopolysaccharide induced RIPK3/MLKL-mediated necroptosis of oral epithelial cells and the further regulation in macrophage activation. Journal of Oral Microbiology 14(1): 2041790. https://doi.org/10.1080/20002297.2022.2041790.
33. Saeed, W.K., D.W. Jun, K. Jang, J.H. Oh, Y.J. Chae, J.S. Lee, D.H. Koh, and H.T. Kang. 2019. Decrease in fat de novo synthesis and chemokine ligand expression in non-alcoholic fatty liver disease caused by inhibition of mixed lineage kinase domain-like pseudokinase. Journal of Gastroenterology and Hepatology 34(12): 2206–2218. https://doi.org/10.1111/jgh.14740.
34. Deuis, J.R., L.S. Dvorakova, and I. Vetter. 2017. Methods used to evaluate pain behaviors in rodents. Frontiers in Molecular Neuroscience 10: 284. https://doi.org/10.3389/fnmol.2017.00284.
35. Hori, T., T. Oka, M. Hosoi, M. Abe, and K. Oka. 2000. Hypothalamic mechanisms of pain modulatory actions of cytokines and prostaglandin E2. Annals of the New York Academy of Sciences 917: 106–120. https://doi.org/10.1111/j.1749-6632.2000.tb05375.x.
36. Buharalioglu, K., O. Ozbasoglu, B. Korkmaz, T. Cuez, S. Sahan-Firat, A. Yalcin, and B. Tunctan. 2009. Thalidomide potentiates analgesic effect of COX inhibitors on endotoxin-induced hyperalgesia by

modulating TNF-α, PGE and NO synthesis in mice. FASEB J 23: 742.4.

37. Cagli, A., S.P. Senol, M. Temiz-Resitoglu, D.S. Guden, A.N. Sari, S. Sahan-Firat, and B. Tunctan. 2021. Soluble epoxide hydrolase inhibitor trifluoromethoxyphenyl-3-(1-propionylpiperidin-4-yl)urea prevents hyperalgesia through regulating NLRC4 inflammasome-related pro-inflammatory and anti-inflammatory signaling pathways in the lipopolysaccharide-induced pain mouse model. Drug Development Research 82: 815–825. https://doi.org/10.1002/ddr.21786.
38. Dolunay, A., S.P. Senol, M. Temiz-Resitoglu, D.S. Guden, A.N. Sari, S. Sahan-Firat, and B. Tunctan. 2017. Inhibition of NLRP3 inflammasome prevents LPS-Induced inflammatory hyperalgesia in mice: contribution of NF-κB, caspase-1/11, ASC, NOX, and NOS isoforms. Inflammation 40: 366–386. https://doi.org/10.1007/s10753-016-0483-3.
39. Senol, S.P., M. Temiz-Resitoglu, D.S. Guden, A.N. Sari, S. Sahan-Firat, and B. Tunctan. 2021. Suppression of TLR4/MyD88/TAK1/NF-kB/COX-2 signaling pathway in the central nervous system by bexarotene, a selective RXR agonist, prevents hyperalgesia in the lipopolysaccharide-induced pain mouse model. Neurochemical Research 46: 624–637. https://doi.org/10.1007/s11064-020-03197-7.
40. Tunctan, B., E. Ozveren, B. Korkmaz, C.K. Buharalioglu, L. Tamer, U. Degirmenci, and U. Atik. 2006. Nitric oxide reverses endotoxin-induced inflammatory hyperalgesia via inhibition of prostacyclin production in mice. Pharmacological Research 53: 177–192. https://doi.org/10.1016/j.phrs.2005.10.009.
41. Bahceli, O., S.P. Senol, M. Temiz-Resitoglu, M.F. Horat, S. Sahan-Firat, and B. Tunctan. 2022. Bexarotene ameliorates LPS-induced hyperalgesia: contribution of TLR4/MyD88-dependent pro-inflammatory, anti-apoptotic, and anti-inflammatory signaling pathways. International Journal of Pharmacology May 31. https://doi.org/10.3923/ijp.2022.XX.XX.
42. Turner, R.A. 1965. *Screening Methods in Pharmacology*. New York: Academic Press.
43. Festing, M.F. 2018. On determining sample size in experiments involving laboratory animals. Laboratory Animals 52(4): 341–350. https://doi.org/10.1177/0023677217738268.
44. Lv, Z., C. Liu, M. Zhai, Q. Zhang, J. Li, F. Zheng, and M. Peng. 2018. LPS pretreatment attenuates cerebral ischaemia/reperfusion ınjury by inhibiting inflammation and apoptosis. Cellular Physiology and Biochemistry 45(6): 2246–2256. https://doi.org/10.1159/000488170.
45. Mitchell, J., S.J. Kim, C. Howe, S. Lee, J.Y. Her, M. Patel, G. Kim, J. Lee, E. Im, and S.H. Rhee. 2022. Chronic intestinal inflammation suppresses brain activity by inducing neuroinflammation in mice. American Journal of Pathology 192(1): 72–86. https://doi.org/10.1016/j.ajpath.2021.09.006.
46. Xie, Y., S. Zhu, M. Zhong, M. Yang, X. Sun, J. Liu, G. Kroemer, M. Lotze, H.J. Zeh, R. Kang, and D. Tang. 2017. Inhibition of aurora kinase A induces necroptosis in pancreatic carcinoma.*Gastroenterology* 153(5): 1429–1443.e5. https://doi.org/10.1053/j.gastro.2017.07.036.
47. Cruz, S.A., Z. Qin, A.F.R. Stewart, and H.H. Chen. 2018. Dabrafenib, an inhibitor of RIP3 kinase-dependent necroptosis, reduces ischemic brain injury. Neural Regeneration Research 13(2): 252–256. https://doi.org/10.4103/1673-5374.226394.

48. Kondo, T., S. Macdonald, C. Engelmann, A. Habtesion, J. Macnaughtan, G. Mehta, R.P. Mookerjee, N. Davies, M. Pavesi, R. Moreau, P. Angeli, V. Arroyo, F. Andreola, and R. Jalan. 2021. The role of RIPK1 mediated cell death in acute on chronic liver failure. Cell Death and Disease 13(1): 5. https://doi.org/10.1038/s41419-021-04442-9.
49. Liu, Y.L., C.C. Hsu, H.J. Huang, C.J. Chang, S.H. Sun, and A.M. Lin. 2020. Gallic acid attenuated LPS-induced neuroinflammation: protein aggregation and necroptosis. Molecular Neurobiology 57(1): 96–104. https://doi.org/10.1007/s12035-019-01759-7.
50. Suda, J., L. Dara, L. Yang, M. Aghajan, Y. Song, N. Kaplowitz, and Z.X. Liu. 2016. Knockdown of RIPK1 Markedly Exacerbates murine immune-mediated liver ınjury through massive apoptosis of hepatocytes, independent of necroptosis and inhibition of NF-κB. Journal of Immunology 197(8): 3120–3129. https://doi.org/10.4049/jimmunol.1600690.
51. Wang, J., Y. Luan, E.K. Fan, M.J. Scott, Y. Li, T.R. Billiar, M.A. Wilson, Y. Jiang, and J. Fan. 2021. TBK1/IKKε negatively regulate LPS-induced neutrophil necroptosis and lung inflammation. Shock 55(3): 338–348. https://doi.org/10.1097/SHK.0000000000001632.
52. Ito, T., K. Yoshida, T. Negishi, M. Miyajima, H. Takamatsu, H. Kikutani, A. Kumanogoh, and K. Yukawa. 2014. Plexin-A1 is required for Toll-like receptor-mediated microglial activation in the development of lipopolysaccharide-induced encephalopathy. International Journal of Molecular Medicine 33(5): 1122–1130. https://doi.org/10.3892/ijmm.2014.1.690.
53. Chang, E.Y., J. Zhang, S. Sullivan, R. Newman, and I. Singh. 2011. N-acetylcysteine attenuates the maternal and fetal proinflammatory response to intrauterine LPS injection in an animal model for preterm birth and brain injury. Journal of Maternal-Fetal and Neonatal Medicine 24(5): 732–740. https://doi.org/10.3109/14767058.2010.528089.
54. Huang, P., X. Chen, X. Hu, Q. Zhou, L. Lin, S. Jiang, H. Fu, Y. Xiong, H. Zeng, M. Fang, C. Chen, and Y. Deng. 2020. Experimentally induced sepsis causes extensive hypomyelination in the prefrontal cortex and hippocampus in neonatal rats. Neuromolecular Medicine 22(3): 420–436. https://doi.org/10.1007/s12017-020-08602-6.
55. Huang, P., Q. Zhou, Q. Lin, L. Lin, H. Wang, X. Chen, S. Jiang, H. Fu, and Y. Deng. 2020. Complement C3a induces axonal hypomyelination in the periventricular white matter through activation of WNT/β-catenin signal pathway in septic neonatal rats experimentally induced by lipopolysaccharide. Brain Pathology 30(3): 495–514. https://doi.org/10.1111/bpa.12798.

Figures

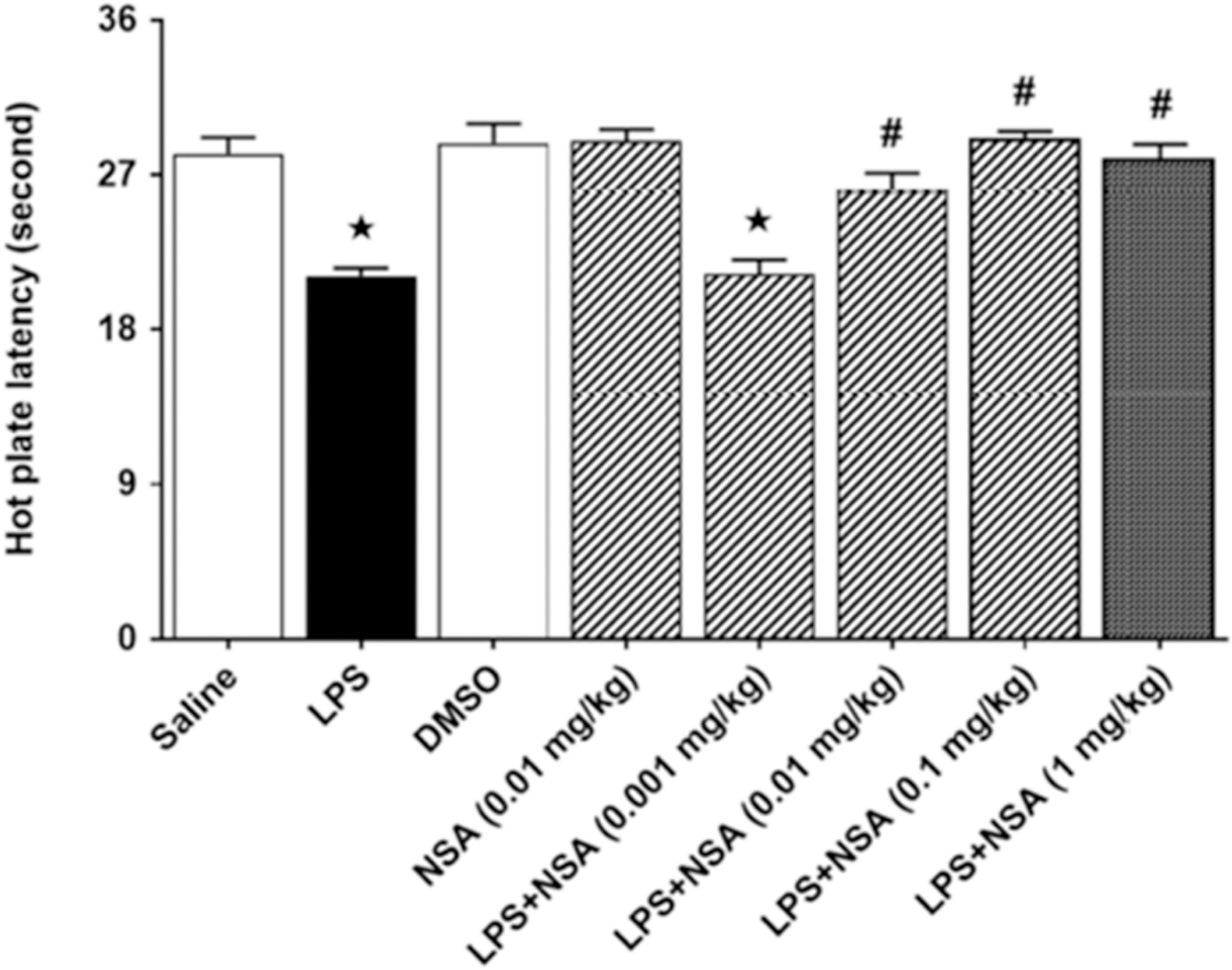

Figure 1

Effect of NSA on LPS-induced hyperalgesia. Response time to thermal stimuli within 30 seconds was determined 6 hours after injection of saline (10 ml/kg, i.p.), LPS (10 mg/kg, i.p.), DMSO (10 ml/kg, i.p.), or NSA (0.001, 0.01, 0.1, or 1 mg/kg, i.p.) in mice using the hot plate test. Data are expressed as means ± SEM from 5-10 animals. $^{*}p < 0.05$ vs. saline-injected group, $^{\#}p < 0.05$ vs. LPS-injected group.

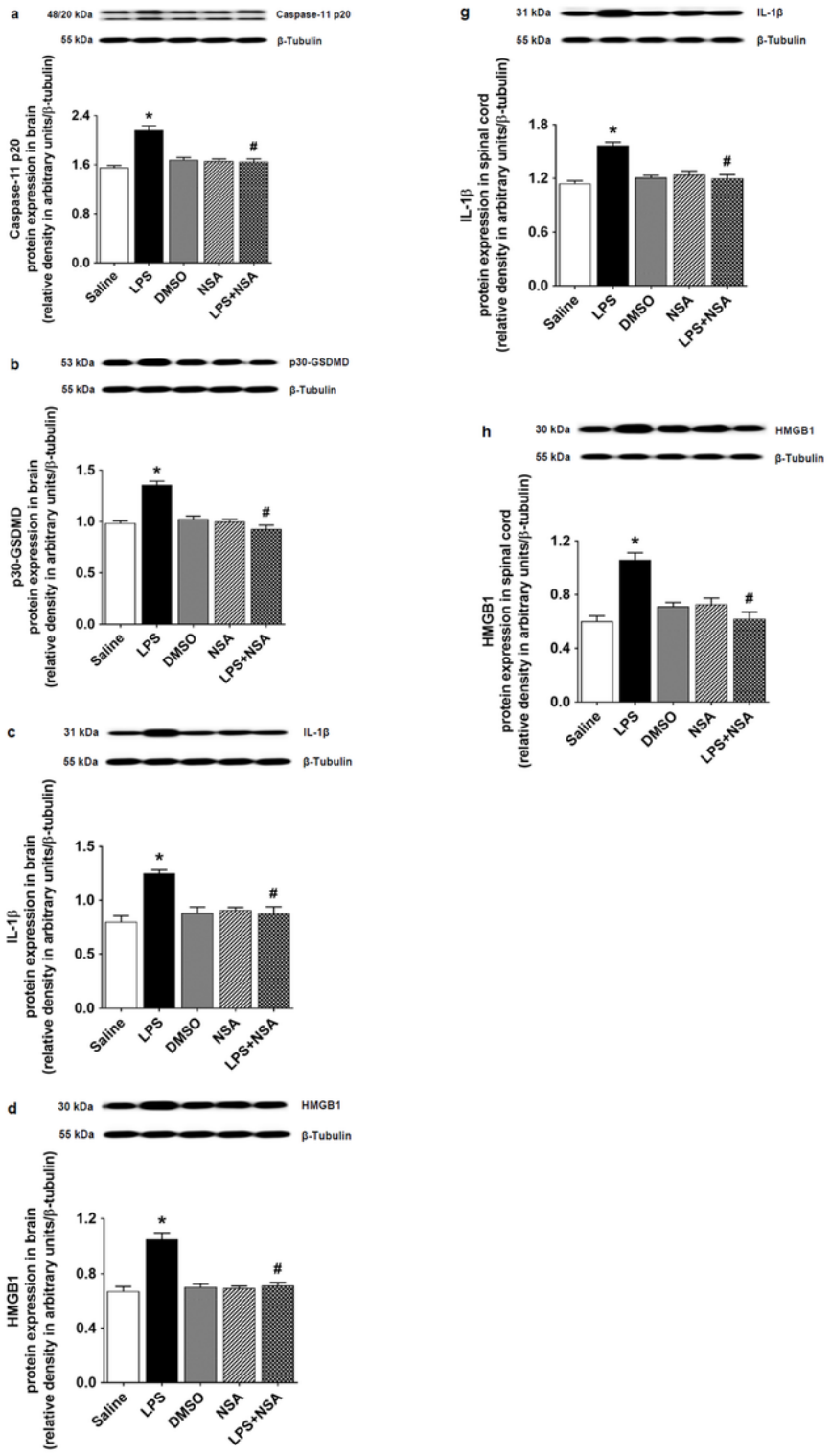

Figure 2

Effect of NSA on LPS-induced increase in caspase-11 p20, p30-GSDMD, IL-1β, and HMGB1 expression in (**a**, **b**, **c**, and **d**, respectively) brains and (**e**, **f**, **g**, and **h**, respectively) spinal cords measured 6 hours after saline (10 ml/kg, i.p.), LPS (10 mg/kg, i.p), DMSO (10 ml/kg, i.p.), or NSA (0.01 mg/kg, i.p.) injection into mice. Caspase-11 p20, p30-GSDMD, IL-1β, and HMGB1 protein expression in tissues was measured using immunoblotting. The samples containing 30 mg of total protein were subjected to an SDS-PAGE (10%).

Data are expressed as means ± SEM from 4 animals. $^{*}p < 0.05$ vs. saline-injected group, $^{\#}p < 0.05$ vs. LPS-injected group.

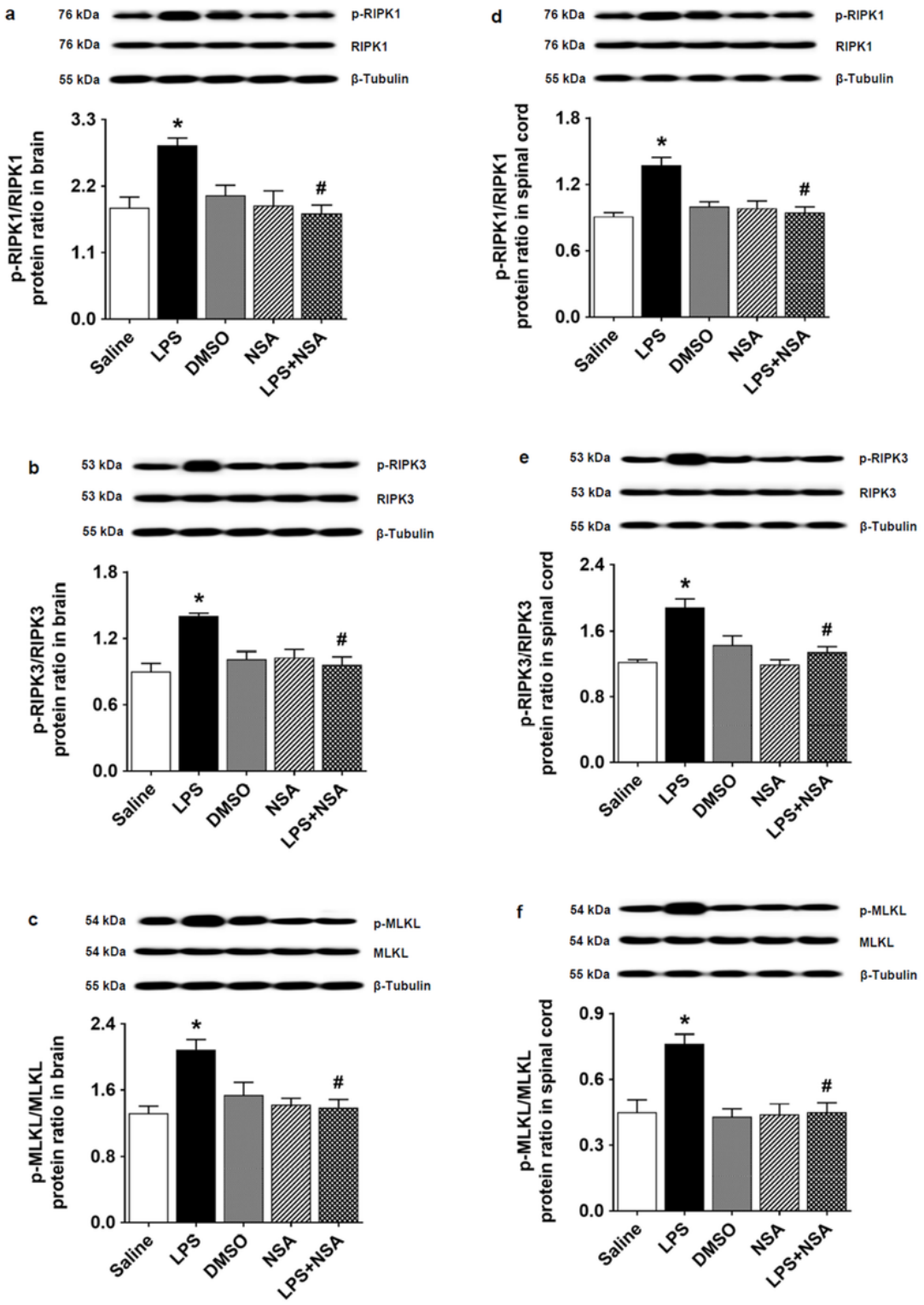

Figure 3

Effect of NSA on LPS-induced increase in RIPK1, RIPK3, and MLKL activity in (**a**, **b**, and **c**, respectively) brains and (**d**, **e**, and **f**, respectively) spinal cords measured 6 hours after saline (10 ml/kg, i.p.), LPS (10 mg/kg, i.p), DMSO (10 ml/kg, i.p.), or NSA (0.01 mg/kg, i.p.) injection into mice. The expression of unphosphorylated and phosphorylated proteins for RIPK1, RIPK3, and MLKL in tissues was measured using immunoblotting. The samples containing 30 mg of total protein were subjected to an SDS-PAGE (10%). Data are expressed as means ± SEM from 4 animals. $^{*}p < 0.05$ vs. saline-injected group, $^{\#}p < 0.05$ vs. LPS-injected group.

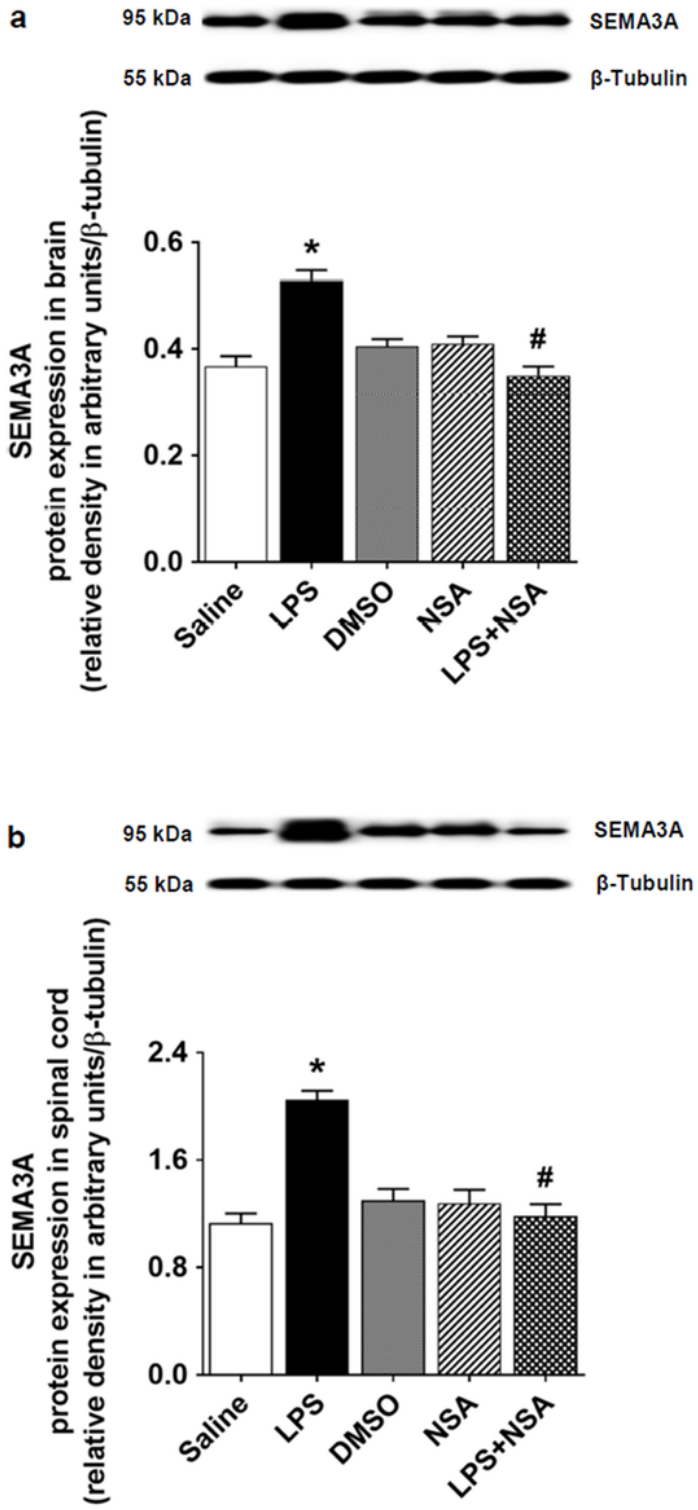

Figure 4

Effect of NSA on LPS-induced increase in SEMA3A expression in (**a**) brains and (**b**) spinal cords measured 6 hours after saline (10 ml/kg, i.p.), LPS (10 mg/kg, i.p), DMSO (10 ml/kg, i.p.), or NSA (0.01 mg/kg, i.p.) injection into mice. SEMA3A protein expression in tissues was measured using immunoblotting. Data are expressed as means ± SEM from 4 animals. $^{*}p < 0.05$ vs. saline-injected group, $^{\#}p < 0.05$ vs. LPS-injected group.

Figure 5

Effect of NSA on LPS-induced decrease in myelin PLP expression in (**a**) brains and (**b**) spinal cords measured 6 hours after saline (10 ml/kg, i.p.), LPS (10 mg/kg, i.p), DMSO (10 ml/kg, i.p.), or NSA (0.01 mg/kg, i.p.) injection into mice. Myelin PLP protein expression in tissues was measured using immunoblotting. Data are expressed as means ± SEM from 4 animals. $^{*}p < 0.05$ vs. saline-injected group, $^{\#}p < 0.05$ vs. LPS-injected group.

Figure 6

See image above for figure legend